Thin Solid Films 612 (2016) 22–28

Contents lists available at ScienceDirect

Thin Solid Films

journal homepage: www.elsevier.com/locate/tsf

$Cu_{2-x}S$ films as counter-electrodes for dye solar cells with ferrocene-based liquid electrolytes

M. Congiu [a,*], O. Nunes-Neto [a], M.L. De Marco [c], D. Dini [c], C.F.O. Graeff [a,b]

[a] UNESP, Univ. Estadual Paulista, POSMAT — Programa de Pós-Graduação em Ciência e Tecnologia de Materiais, Av. Eng. Luiz Edmundo Carrijo Coube14-01, 17033-360 Bauru, SP, Brazil
[b] DC-FC, UNESP, Univ. Estadual Paulista, Av. Eng. Luiz Edmundo Carrijo Coube14-01, 17033-360 Bauru, SP, Brazil
[c] University of Rome "La Sapienza", Department of Chemistry, Piazzale Aldo Moro 5, Rome, RM, Italy

ARTICLE INFO

Article history:
Received 9 August 2015
Received in revised form 16 May 2016
Accepted 19 May 2016
Available online 24 May 2016

Keywords:
Copper sulphide
Solar energy
Counter-electrodes
Ferrocene
Dye solar cells
Semiconductors

ABSTRACT

In this work, the application of hexagonal CuS nanoparticle layers as counter electrodes for dye sensitized solar cells has been studied. A fast, cheap and reliable deposition method was proposed for the one-step preparation of $Cu_{2-x}S$ layers on F-doped SnO_2 within 30 min through an ink-based technique. The electrodes prepared with our method were tested with iodine/iodide electrolyte, Co(II)/(III) bipyridine redox shuttle and Fe(II)/(III) ferrocene-based liquid electrolyte. The $Cu_{2-x}S$ layers showed high efficiency and stability with the ferrocene/ferrocenium redox couple, showing a fast charge recombination kinetic, low charge transfer resistance ($R_{ct} = 0.73\ \Omega\ cm^2$), reasonably high limiting current (11.8 mA cm^{-2}) and high stability in propylene carbonate.

1. Introduction

The search for more efficient and cheaper materials is a fundamental part of research on renewable energy. In this direction, efforts have been made in the two decades following the discovery of the modern version of dye sensitized solar cell (DSSC) also known as Grätzel cell [1,2]. This type of solar cell has proved to be very promising owing to its cheaper costs, ease of fabrication and its high efficiencies up to 13% [3]. However, one of the biggest problems of DSSCs is long-term stability, due mainly to the use of a liquid electrolyte. Furthermore, the most commonly used liquid electrolyte is based on the I^-/I_3^- redox couple which is reactive in nature leading to degradation of the components of the cell. For example, traces of water catalyze the formation of the ion IO_3^-, which contributes to the bleaching of the dye into the device [4,5]. Iodine, along with 3-methoxyproprionitrile (3-MPN), can also participate in other degradation processes leading to the formation of solid electrolyte interfaces [6] and the depletion of thiocyanate ligands of the dye [7,8]. Actually good alternatives to the iodine-based electrolytes do exist, such as cobalt (II)/(III) polypyridine complexes [9–11] and ferrocene [12]. Such redox couples are less reactive than I^-/I_3^- and thus are very interesting to improve the long-term stability of the device. Another important part of the DSSC is the counter electrode (CE). This part of the cell, in a common n-type device, is responsible for the reduction (cathode) of the oxidized redox mediator. A typical CE for DSSC consists of transparent layer of deposited platinum (Pt) nanoparticles on F-doped tin oxide (FTO) [13,14]. However, Pt is a scarce and expensive material and its use can significantly influence the overall cost of the device. Other efficient and cheap materials can be used for the fabrication of CEs such as carbon nanotubes [15,16], graphene [17] and transition metals sulphides [18–20]. The latter is very promising for the production of low-cost solar cell devices owing to their high abundance and ease of production. For example cobalt sulphide (CoS) has been studied and applied in DSSC with iodine-based liquid electrolytes resulting in good efficiency and stability in comparison to Pt [19,21,22]. In our two recent works, we have shown the potential use of CoS CEs with iodine-free electrolytes for both DSSC and quantum-dots sensitized solar cells (QDSSCs) [19,23]. However, cobalt is a heavy and relatively toxic metal and its presence, along with other inorganic pollutants, is strictly monitored in drinking water, in food and in soils, in many industrialized countries. Another interesting material for solar energy is copper sulphide (CuS). CuS is p-type semiconductors with a direct band gap energy ranging from 0.6 to 2.35 eV depending on crystal structure and stoichiometry [24]. CuS forms five stable phases: covellite (CuS), anilite ($Cu_{1.75}S$), digenite ($Cu_{1.8}S$), djurleite ($Cu_{1.95}S$) and chalcocite (Cu_2S). $Cu_{2-x}S$ have been largely used in heterojunction solar cells combined with CdS since 1952 [25]. In the field of sensitized solar cells, CuS has been used for the production of QDSSCs CEs [26–28]. Hereby we propose ($Cu_{2-x}S$) nano-crystals thin films as active and catalytic layer for the simplest and cheapest preparation of high efficient CEs for DSSCs

* Corresponding author.
E-mail address: mirko.congiu@fc.unesp.br (M. Congiu).

http://dx.doi.org/10.1016/j.tsf.2016.05.033
0040-6090/

and QDSSCs, showing the advantages and limitations of this material with different redox liquid electrolytes.

2. Materials and methods

Copper(II) chloride ($CuCl_2 \cdot 2H_2O$); acetylacetone (acac); sodium hydroxide (NaOH); 2,2-bipyridyl; tioacetamide (TAA) ammonium hexachlorophosphate (NH_4PF_6); hydrogen peroxide (H_2O_2 30% solution); dichloromethane (CH_2Cl_2); acetonitrile (ACN); isopropanol (IPA); ammonium hydroxide; F-doped tin oxide glass slides (~7 Ω/□); acetone and absolute ethanol (EtOH) were provided by Sigma-Aldrich. High stability I^-/I_3^- electrolyte (HSE) was provided by Dyers, Rome-Italy. Electrochemical Impedance Spectroscopy (EIS) and current versus potential analysis were performed using a MetrohmAutolabPGStat 330. The EIS spectra were registered in the dark using a single sine waveform with amplitude of 10 mV and a fixed offset of 0.0 V, from 100 kHz to 10 mHz. X-Ray diffraction (XRD) patterns were collected with a diffractometer DMAX Ultima (Rigaku International Corporation, Tokyo, Japan) using $CuK_{\alpha 1}$ radiation, operating at 40 kV and 20 mA. Scans were performed from 5° to 80° with a step size of 0.02° with a scan speed of 2°/min. The morphology of the CEs was investigated through atomic force microscopy (AFM) using a Park Systems XE7 microscope. The measurements were performed in contact mode scan in X,Y direction to avoid artifacts. Using a tip: 0.2 N/m, resonance frequency 23 kHz, PPP-CONSTCR Nanosensors, tip radius <10 nm.

CuS hexagonal stacked plates have been prepared following the method proposed by Busuet al. [29]. Briefly, a solution 0.1 M of $Cu(acac)_2$ in DCM was prepared dissolving the copper complex in the solvent by sonication. In a test tube, 2.5 mL of the as prepared solution was then transferred and 1.25 mL of 0.2 M TAA and 1.25 mL of 0.2 M NaOH were added. The tube was screw capped and the reaction was let to take place during 4 h heating the tube under a 100 W light bulb. After 4 h, the particles which formed at the liquid-liquid interface, were extracted, washed with methanol and dissolved in absolute ethanol by sonication (5 mg/mL). A deep green suspension was then obtained. The square 2 × 2 cm FTO substrates were cleaned by the RCA process, using a bath of water, H_2O_2 and ammonium hydroxide (5:1:1 v:v:v) followed by a bath of water, H_2O_2 and HCl (5:1:1 v:v:v) at 70 °C for 15 min. Then, the cleaned FTO substrates were rinsed with isopropyl alcohol. The FTO substrates were heated at 200 °C on a laboratory hot plate, then 150 μL of CuS ethanol suspension was rapidly dropped on the substrate. The rapid evaporation of ethanol produced a transparent-green layer of CuS. The as deposited CuS films were annealed during 240 min at 200 °C.

The cobalt polypyridine $[Co(byp)_3]^{2+/3+}$ complexes were synthesized as follows: 1 equiv of $CoCl_2 \cdot 6H_2O$ and 3.3 equiv of the polypyridine ligand were dissolved in a minimal amount of methanol, and the solution was stirred at reflux for 2 h. An excess of ammonium hexafluorophosphate was then added to the solution to precipitate the compound that was filtered, washed with methanol and ethanol, dried under vacuum, and used without further purification. The oxidation of the Co(II) complex was performed using an excess of H_2O_2 and concentrated HCl (1:1 v:v). The oxidized complex was precipitated and washed several times with methanol and ethanol. After the synthesis, the cobalt complexes were used to prepare the cobalt liquid electrolyte (CoLE). The electrolyte was prepared dissolving the complexes in a mixture of ACN and methoxyproprionitrile (MPN) 30:70 v:v 0.1 M $[Co(byp)_3]^{2+}$ and 0.05 M $[Co(byp)_3]^{3+}$. The ferrocene electrolyte (FCE) was prepared dissolving 0.1 M of ferrocene and 0.05 M of ferrocenium tetrafluoroborate in propylene carbonate. In order to minimize the contact with atmospheric oxygen, due to the degradation of ferrocenium ion, the solution was kept inside a glove box, under nitrogen atmosphere. Dummy cells were fabricated using two CuS CEs sealed facing one another using a 25 μm hotmelt Bynel® spacer. The mask had been cut, leaving a square chamber (0.5 cm^2), connected to the outside through a small hole in the polymer. The sealing was performed at 150 °C and the electrolytes (FCE, CoLE and HSE) were injected by vacuum backfilling using the small hole left in the mask polymer. The hole was then closed using a piece of Bynel®. In order to study the stability of dummy cells, the electrochemical parameters were monitored as a function of time on devices exposed to sun light soaking, ageing in the dark and consecutive CV cycles (20 mV s^{-1}) from −1.0 to 1.0 V.

3. Results

The characterization of the crystal structure of CuS thin films was performed through XRD measurements, directly on the surface of the CEs. The patterns obtained were compared with those contained in the JCPDS database. The characteristic diffraction peaks of hexagonal covellite (CuS, 79–2321), hexagonal digenite ($Cu_{1.8}S$, 47–1748) and orthorhombic djurleite ($Cu_{1.97}S$, 20–0365), are shown in Fig. 1.

Fig. 1 shows the effect of the annealing time on the characteristics of the CuS layers deposited on FTO. Notice that, as confirmed form XRD patterns, increasing the annealing time the films become more crystalline. A non-stoichiometric crystal phase of ($Cu_{2-x}S$) was detected, due to the coexistence, in the material, of both Cu^{2+} and Cu^+. A longer annealing time (240 min) also improves the adherence of the films to the substrate. This was observed by scratching the film using a metal blade.

The AFM images of the CEs surface are shown in Fig. 2 with two different magnifications. The CE presented a rough surface, uniformly covered by CuS nanoparticles without any fractures.

Symmetric dummy cells were characterized through cyclic voltammetry in order to determine the reversibility of the liquid electrolytes and the limiting currents (I_L). Dummy cells with Pt CEs were used as reference. As shown in Fig. 3(B), just the Fc/Fc^+ redox couple shows good charge transfer characteristics with $Cu_{2-x}S$ CEs. In fact, the $[Co(byp)_3]^{2+/3+}$ curve is asymmetric within the considered overpotential window (from −1.0 V to 1.0 V) and thus the redox reaction is probably irreversible. I^-/I_3^- redox couple, resulted not suitable for application with $Cu_{2-x}S$ CEs. In fact, as shown in Fig. 4, a little drop of HSE can rapidly dissolve the $Cu_{2-x}S$ layer causing an irreversible damage to the CE. On the other hand, all of the redox electrolytes show a good reversibility using Pt CEs.

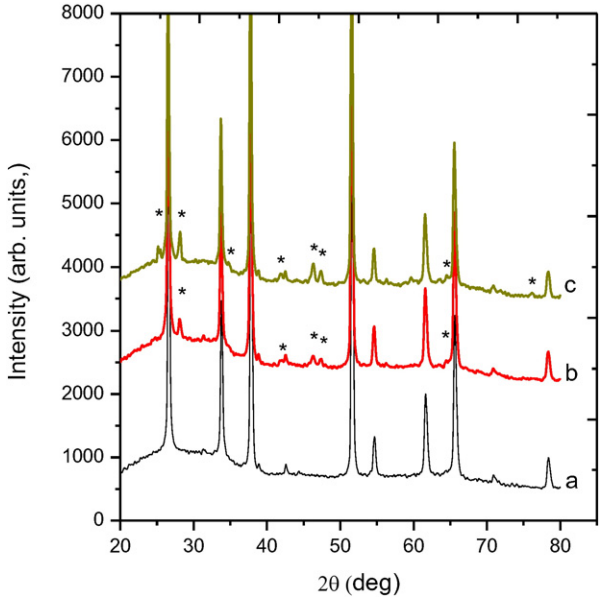

Fig. 1. XRD patterns of the FTO substrate (a) and CuS (*) thin films annealed at 200 °C for 30 (b) and 240 (c) minutes. In the diffraction spectra (b) and (c) it is possible to see the peaks characteristic of a $Cu_{2-x}S$ phase, composed by a mixture of covellite CuS (79–2321), digenite ($Cu_{1.8}S$, 47–1748) and djurleite ($Cu_{1.97}S$, 20–0365). JCPDS database.

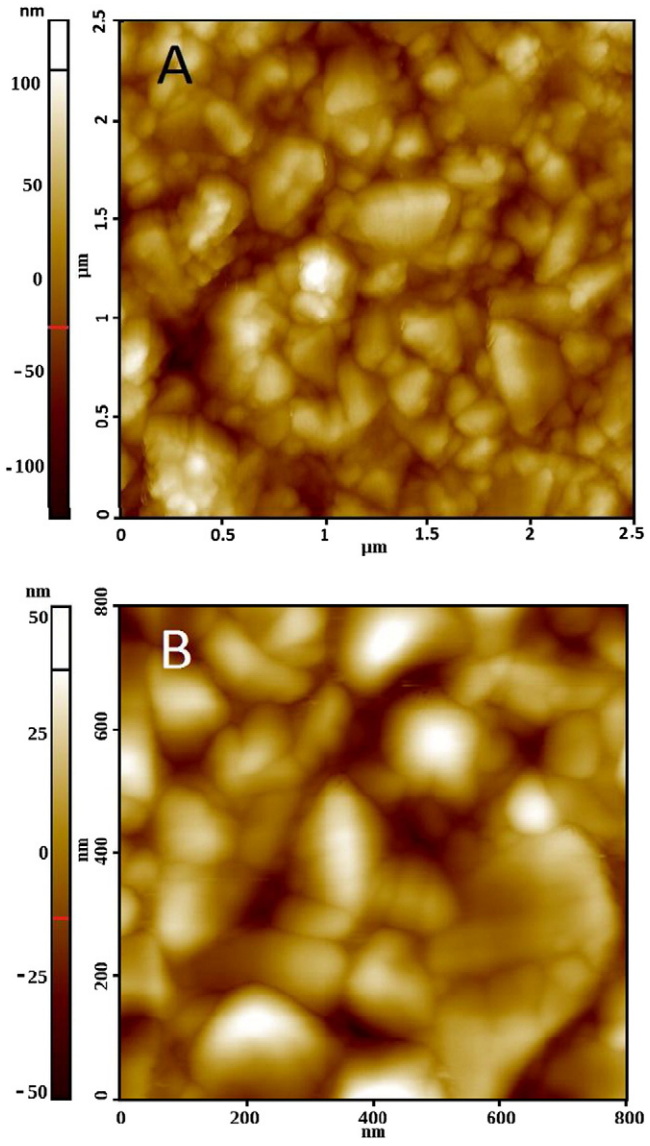

Fig. 2. AFM images of the surface of the CuS CEs. The two images represent two different magnifications of the same region considering in (A) 6.26 and in (B) 0.64 μm^2.

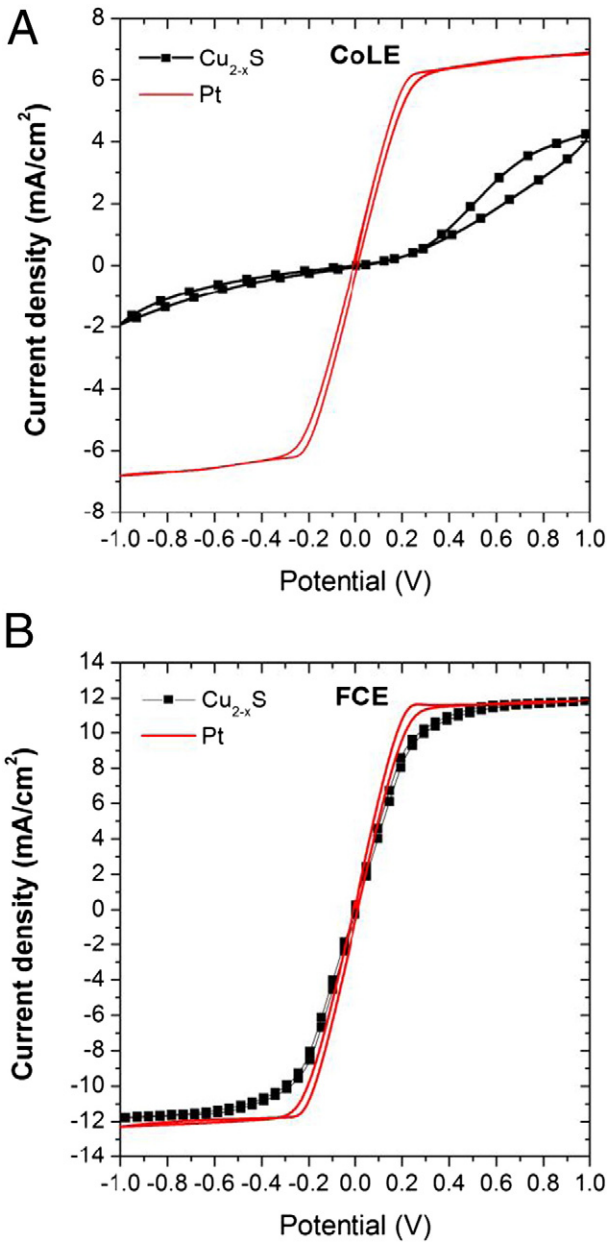

Fig. 3. Cyclic voltammetry response of dummy cells filled with CoLE (A) and FCE (B). The current vs voltage response of $Cu_{2-x}S$ (-■-) CEs have been compared with that of Pt (red continuous line).

The values of the I_L for FCE obtained with $Cu_{2-x}S$ and Pt CEs were respectively 11.8 ± 0.5 and 12.2 ± 0.4 mA cm^{-2}. The value of the I_L calculated for CoLE was 6.8 ± 0.4 mA cm^{-2} using Pt as CE. In Fig. 3 one can see that the curve of FCE, using CuS CEs, has smaller currents compared to Pt on the same potential.

EIS has been used in order to study the recombination kinetics and understand the different contribution of the resistive and capacitive components of the dummy cell. The impedance spectra have been fitted using a Randles equivalent circuit. In Fig. 5 one can see the different electrochemical responses of both Pt and $Cu_{2-x}S$ CEs with FCE (a) and CoLE (b).

In the Nyquist plot using Pt and CoLE (Fig. 5) the charge transfer kinetic associated to the $[Co(byp)_2]^{2+/3+}$ redox couples showed a value of R_{ct} of 0.13 Ω cm^2 and a capacitance of 38.10 μF/cm^2. $Cu_{2-x}S$ CE, using the same electrolyte, shows high charge transfer resistance, 935.30 Ω cm^2. The capacitance calculated for the dummy cells with $Cu_{2-x}S$ CEs and CoLE was 3.13 μF/cm^2. The charge transfer resistance associated to the $Fc^{(0)}/Fc^{(+1)}$ redox couple (Fe^{2+}/Fe^{3+}) was 0.73 Ω cm^2 with a capacitance of 23.4 μF/cm^2. As one can see in the Nyquist plot referred to the FCE, the EIS response of the dummy cells made with Pt CEs presents just a diffusive behaviour. The diffusion resistance was calculated by fitting using a Warburg finite length diffusion element (W_s) [30]. For Pt in FCE, the real part of the Warburg diffusion resistance (W_R) was 17.9 Ω while the Warburg time constant (W_T) was 4.2 s.

The stability of $Cu_{2-x}S$ CEs was studied by impedance spectroscopy, monitoring the value of R_{ct} for 10 days. In order to determine the effect of light exposure, some cells were left to age under simulated sun light (AM 1.5, 1 sun) while other samples were kept in the dark. In order to compare different samples, R_{ct} was normalized, the value of R_{ct} was then divided by the lowest value for each sample. The results are presented in Fig. 6 for the as-deposited (A) and annealed (B) CEs.

As seen in Fig. 6(A), the unannealed samples show a significant loss in charge transfer efficiency, there is an increase of R_{ct} by about a factor of 8. On the other hand, thermal annealed samples show an increase of

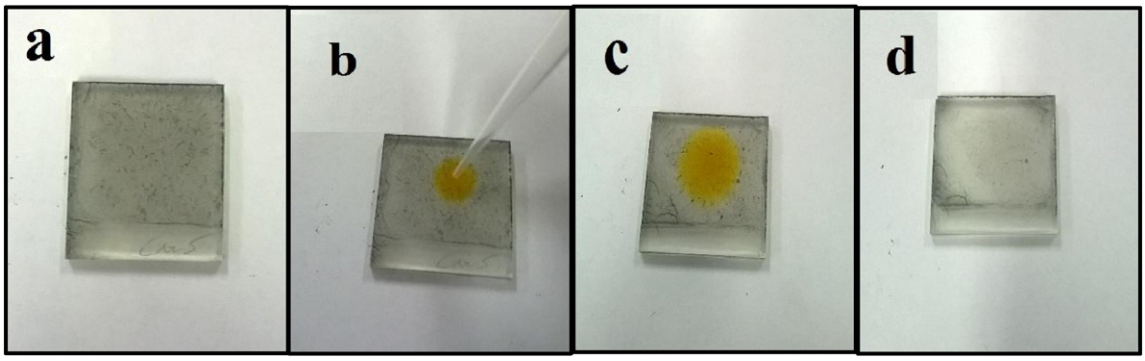

Fig. 4. The corrosion of $Cu_{2-x}S$ electrodes by HSE. On the surface of a $Cu_{2-x}S$ electrode (a) a small drop of the iodine-based HSE is dropped (b). The electrode has been let to react with HSE during 10 min (c), then is washed with absolute ethanol (d).

R_{ct} during the first 150 h, followed by stabilization over the considered time. However, the increase in R_{ct} remains below 50% of the initial value of the overall time of the experiment. As shown in Fig. 6(B), the light exposure has no effect on the evolution of R_{ct}.

In order to evaluate the electrochemical stability of our $Cu_{2-x}S$ CEs, dummy cells filled with FCE have been cycled with CV slow scans (20 mV s^{-1}) from −1.0 to 1.0 V. Fig. 7 shows the evolution of R_{ct} applying successive CV cycles to the dummy cells filled with FCE. After the first 50 cycles, one can observe a reduction of the R_{ct} value. Probably, during the first cycles, the electrolyte starts to penetrate inside the porous $Cu_{2-x}S$ layer, improving the overall efficiency of the charge transfer process at the interface CE/electrolyte. The value of R_{ct} remains below 0.8 Ω cm^2 up to 300 CV cycles.

4. Discussion

In this research work, CuS hexagonal stacked nanoparticles, synthesized through the process proposed by Busu et al. [29], have been deposited on FTO and thermally converted to $Cu_{2-x}S$. The obtained CEs have been considered for use with DSSCs liquid electrolytes such as the iodine based HSE, cobalt(II)/(III) tris-bipyridine redox shuttle and ferrocene. CuS thin films have been deposited on square (2 × 2 cm) FTO substrates by drop casting a suspension of CuS hexagonal nanocrystals in absolute ethanol [29]. As shown in Fig. 1, the material showed diffraction peaks characteristic of three different $Cu_{2-x}S$ phases (JCPDS): hexagonal covellite (CuS, 79–2321), hexagonal digenite ($Cu_{1.8}S$, 47–1748) and orthorhombic djurleite ($Cu_{1.97}S$, 20–0365). The presence of digenite and djurleite is probably due to the low deposition temperature. In fact, it is known that CuS can be thermally converted to Cu_2S. However the absence of chalcocite (Cu_2S) phase in the deposited films is due to its lower stability, under ambient conditions, in comparison with the more stable $Cu_{1.97}S$ phase as reported also by Zhao et al. [31]. The reaction produces $Cu_{2-x}S$ (2,x ≤ 0) intermediate crystal phases. The sulphur depletion reaction (Eqs. (1) and (2)) can occur in vacuum [32], under inert atmosphere [28] and also in the presence of atmospheric oxygen [33,34].

$$2CuS + O_2 \rightarrow Cu_2S + SO_2 \quad (1)$$

$$2CuS \rightarrow Cu_2S + \tfrac{1}{2}S_2 \quad (2)$$

The fast evaporation of ethanol at 200 °C leads to the formation of a semi-transparent CuS film. The as deposited material starts to lose sulphur through reaction (1) that leads to the formation of $Cu_{2-x}S$ phases. In Fig. 1 one can see that the films became more crystalline for longer thermal annealing treatments. This is confirmed by the increase of the intensity of the peaks referred to $Cu_{2-x}S$ phases.

The study of the morphology through AFM imaging showed a rough surface consisting of a uniform layer of CuS nanoparticles. As shown in Fig. 2, the particles are in contact with each other. The roughness (RMS) of the surface have been calculated by processing the AFM images which resulted to 0.439 μm, notice that the typical RMS of commercial FTO is around 20 nm [35]. The presence of nanoparticles increases the surface area of the CE. In order to calculate the surface area of the CE, AFM images were collected on a square region (3 × 3 μm) of the $Cu_{2-x}S$ film. The value of the surface area calculated by processing the AFM images, was 11.3 μm^2, 26% higher than the area of the considered square region (9.0 μm^2). The electrocatalytic activity of $Cu_{2-x}S$ CEs has been investigated using three different electrolytes: CoLE; HSE and FCE. In Fig. 4, one can see the corrosive effect of HSE, which rapidly dissolves the $Cu_{2-x}S$ layer. This occurs also in the dummy cell, for this reason our CEs are not suitable for use with iodine-based electrolytes. This could be due to the high affinity of I^- ions for the Cu(I) atoms, which are present in CuS as observed also by Lefèvre et al. [36].

Cyclic voltammetry and EIS measurements have shown the incompatibility of $Cu_{2-x}S$ CEs with the cobalt-based electrolyte used in this study. In fact, as shown in Fig. 3, the voltammogram of CoLE over CuS resulted asymmetric with a low slope near 0 V. This could be due to a bad charge transfer kinetic at the CEs surface. The asymmetry of the curve shown is probably the result of an irreversible redox reaction involving the $[Co(byp)_3]^{2+}/[Co(byp)_3]^{3+}$ redox couple. EIS analysis confirmed the high charge transfer resistance at 0 V over potential (935.30 Ω cm^2), as shown in Fig. 5. On the other hand, the same electrolyte showed a reversible electrochemical behaviour on Pt CEs, as expected with a fast charge transfer kinetic. According to the Debye model, the time constant (relaxation time) of the system can be calculated from the impedance spectra of our dummy cells, approximated to a parallel RC circuit. The relaxation time of the system (τ) can be written as follows (Eq. (3)):

$$\tau = R_{ct}C_{dl} \quad (3)$$

where R_{ct} is the charge transfer resistance and C_{dl} is the capacitance of the double layer, both calculated by fitting (Fig. 8) the EIS spectrum with Randles equivalent circuit. For CoLE, the value of τ is 4.9 μs for Pt CE and 2.9 ms for $Cu_{2-x}S$. This high difference of relaxation time is due to the higher value of R_{ct} at the $Cu_{2-x}S$//CoLE interface (Fig. 4).

Different from what is seen with CoLE and HSE, $Cu_{2-x}S$ CEs have shown an excellent electro-catalytic activity and stability with FCE. From cyclic voltammetry (Fig. 3) it is possible to observe a symmetric hysteresis of the current/voltage curve, characteristic of reversible redox reactions. Notice that the slope of the curve is very close to that observed using Pt CEs since the high part of the resistance through the cell is given by the diffusion resistance, which depends just on the solvent, temperature and the redox shuttle. As shown in Fig. 5(B), the

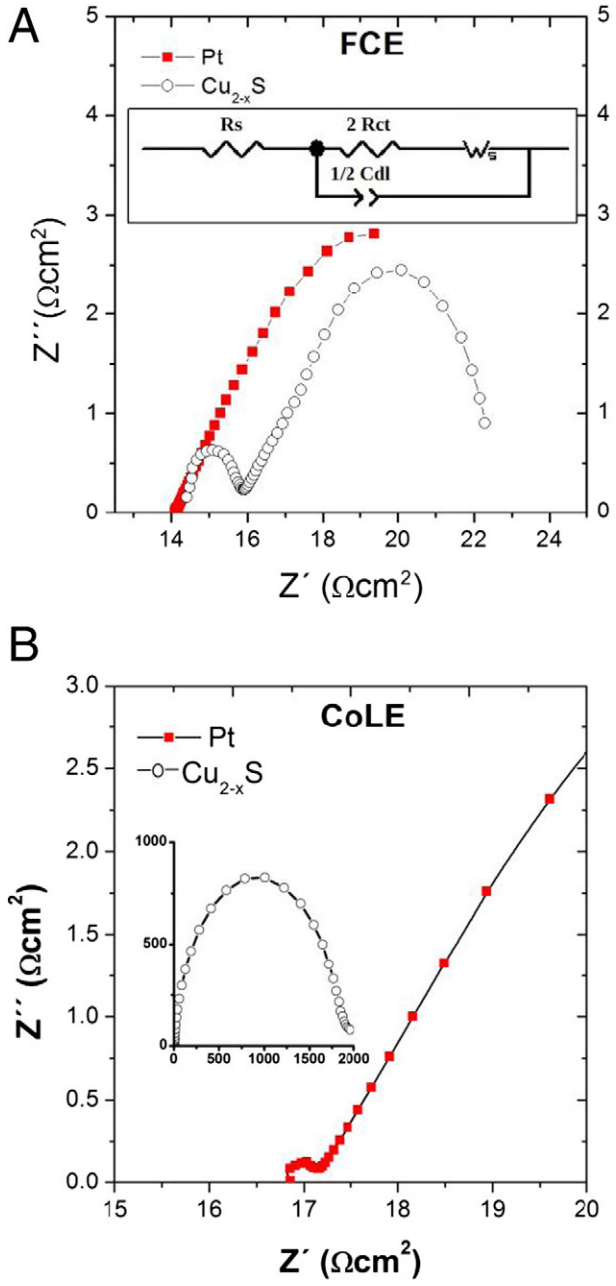

Fig. 5. Nyquist plots of dummy cells with platinum and with $Cu_{2-x}S$ CEs, filled with FCE (a) and CoLE (b). All of the EIS measurements were performed at 0.0 V DC offset. The equivalent circuit used to fit all of the impedance spectra in the insert of (a).

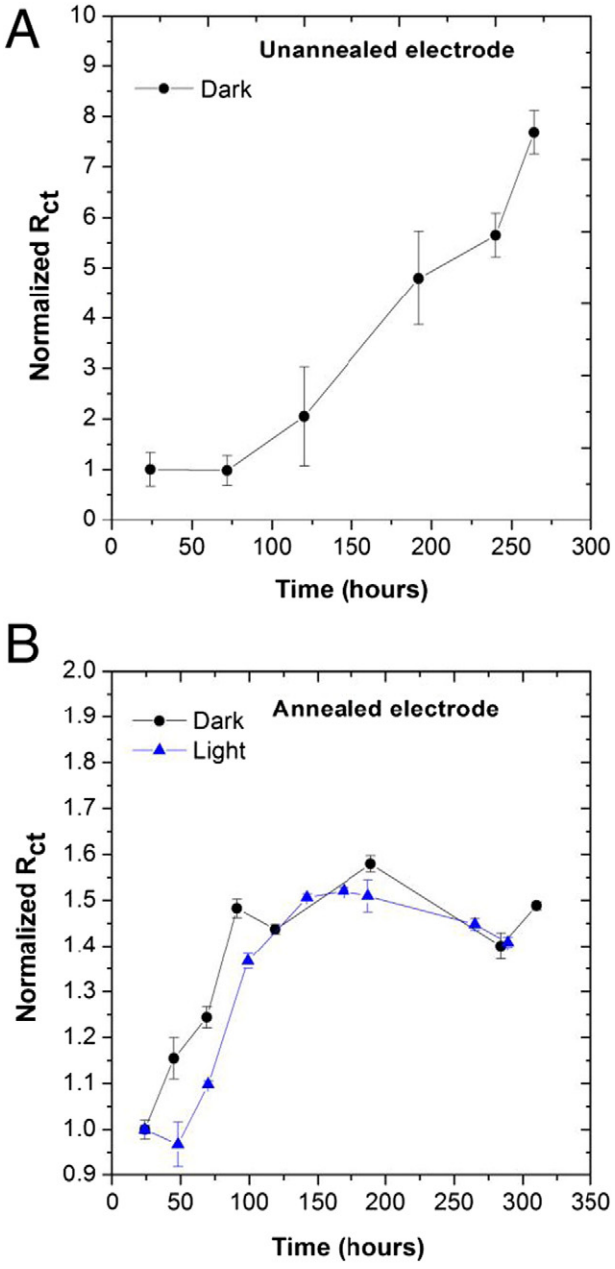

Fig. 6. Time-dependent evolution of charge transfer resistance (R_{ct}) for unannealed (a) and annealed (b) $Cu_{2-x}S$ CEs with FCE. The normalized R_{ct} was calculated normalizing all of the values by the lower.

first semicircle in the Nyquist spectrum, referred to the charge transfer process, presents an amplitude on the real-Z′ axes of just 1.46 Ω cm^2, which corresponds to a value of R_{ct} of 0.73 cm^2. The calculated capacitance of the $Cu_{2-x}S$//FCE dummy cell is 23.4 μF/cm^2, and thus the value of τ is 17.1 μs. Notice that the relaxation time of the commonly used Pt/FTO CEs with a commercial HSE is around 100 μs, showing R_{ct} values around 2 Ω cm^2 [19,37,38]. The Nyquist plot of a dummy cell filled with FCE using two Pt CEs is represented in Fig. 5(A). For this system (Pt//FCE//Pt), the charge transfer impedance is so small that can it be neglected in the fitting model. In fact, the experimental data can be fitted using a circuit composed of a series resistance R_s, which considers the resistance due to the electric contact and a Warburg diffusive element W_s, which considers the impedance resulting from a finite diffusion of the ions through the electrolyte layer between the CEs. It is important to remember that the Warburg diffusion element (W_s) is a constant phase element which presents a constant phase angle of 45°, independent of the frequency (ω). The impedance modulus $|Z_{Ws}|$ of this element is described by Eq. (4):

$$|Z_{Ws}| = \frac{\sqrt{2\sigma}}{\omega^{0.5}} \tag{4}$$

the Warburg constant (σ) is defined by Eq. (5):

$$\sigma = \frac{RT}{n^2F^2A\sqrt{2}}\left(\frac{1}{D_O^{0.5}C_O}\frac{1}{D_R^{0.5}C_R}\right) \tag{5}$$

where n is the number of electrons in the redox reaction, F is the Faraday constant R is the real gas constant, T is the temperature, A is the area of the CE, D_O and D_R are the diffusion coefficients of the oxidized and reduced forms of the species; C_O and C_R are their respective

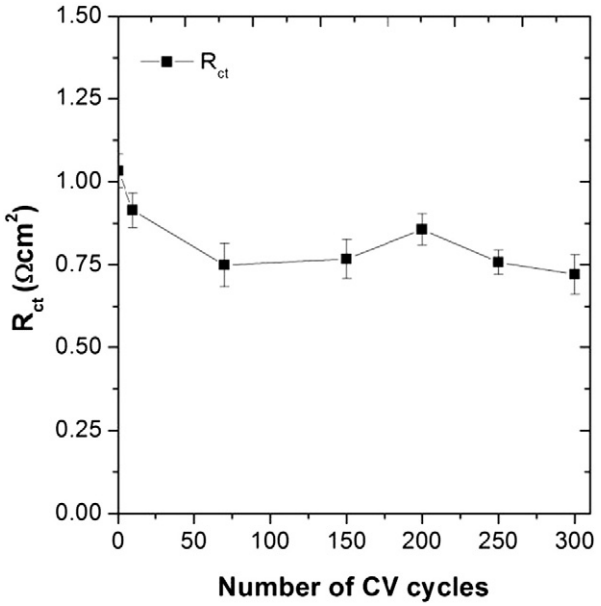

Fig. 7. Evolution of R_{ct} applying continuous CV cycles with a scan rate of 20 mV/s from −1.0 to 1.0 V. Typical dummy cells, with two identical $Cu_{2-x}S$ electrodes, was filled with FCE and used to perform the stress tests, registering the value of R_{ct} through EIS.

concentrations in the electrolyte. Eq. (4) can be written also as (Eq. (6)) [39]:

$$Z_{Ws} = W_R \frac{\tanh\left(\sqrt{i\omega W_T}\right)}{\sqrt{i\omega W_T}} \tag{6}$$

where W_R is the real part of the Warburg impedance (at very low frequency) and W_T is the Warburg time constant, experimentally obtained

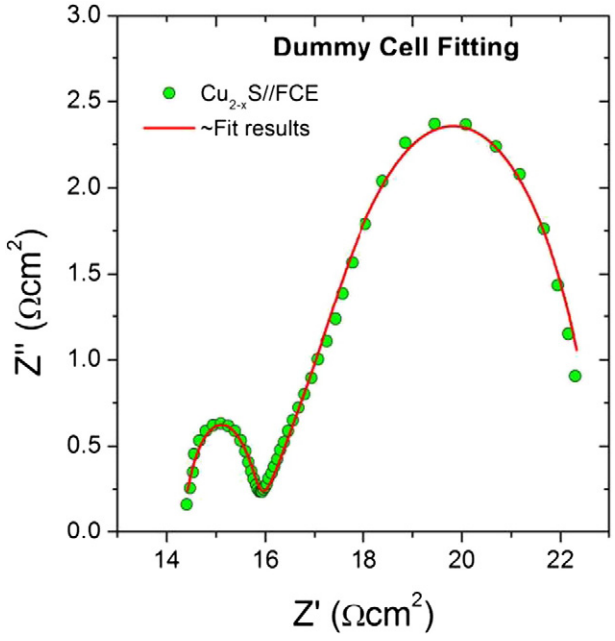

Fig. 8. Results of the fitting of the EIS spectrum (Nyquist plot) of a typical CuS dummy cell filled with FCE. The Randles circuit perfectly fits the experimental data, considering both the charge transfer (first semicircle) kinetics and the diffusion impedance (Warburg diffusion).

by fitting the experimental data. The diffusion coefficient of the redox species can be calculated from W_T, using Eq. (7):

$$D = \frac{L^2}{W_T} \tag{7}$$

the value of W_T obtained for the dummy cell Pt//FCE//Pt was 4.2 s and thus the value of the calculated diffusion coefficient D 1.48×10^{-6} cm^2 s^{-1} considering a diffusion length (L) of 25 μm which corresponds with the thickness of the hot melt spacer used to seal the cell. Notice that D is a value referred to both the oxidized and reduced form of ferrocene (Fc^+/Fc^0). In fact, looking at Eq. (5) one can see that in the Warburg equation, D_O and D_R are multiplied by the respective bulk concentration. The value of W_T and D calculated from Eq. (7) resulted close to the values of ferrocene and ferrocenium in propylene carbonate (the same solvent used in our FCE), calculated by CV measurements in a similar experiment (2.03 and 1.38×10^{-6} cm^2 s^{-1} respectively) [40]. Along with the high electrocatalytic efficiency, $Cu_{2-x}S$ counter CEs have shown also a good stability in dummy cells with FCE when annealed at 200 °C for 240 min. In fact, looking at Fig. 6(a), one can see that there is a significant increase of R_{ct} as a function of time for the unannealed CEs (Fig. 6(B)) while the increase observed for the annealed samples remained below 50% of the initial value. The similar behaviour in the evolution of R_{ct} of the annealed samples in the dark and under illumination suggests that light exposure does not affect the overall performance of the CE. Repeated slow (20 mV s^{-1}) CV cycles from −1.0 V to 1.0 V demonstrate that $Cu_{2-x}S$ is very stable under high electrical stress. In fact, no significant increase in R_{ct} has been observed during the stress-test (Fig. 7). Contrariwise there is an improvement of the performance during the first 50 cycles. This behaviour is common in this kind of experiments and it is probably due to diffusion of the electrolyte inside the pores of the material (i.e. $Cu_{2-x}S$) [41]. In fact, during the first few hours of the life of the device, the electrolyte starts to penetrate deeply inside the porous films, reaching more active sites of the solid catalyst. The electrocatalytic efficiency of our $Cu_{2-x}S$ CEs are very promising in comparison with other similar applications published so far in the literature. An example is the use of a metallic PEDOT as cathode for cobalt-based electrolytes, which shows an interfacial charge transfer resistance of 2.7 Ω cm^2 with a time constant (relaxation time) of 18.03 μs ($R_{ct} \times C_{dl}$) [42]. The system $Cu_{2-x}S$// FCE that we proposed has shown a lower value of R_{ct} of just 0.73 Ω cm^2 with a time constant of 17.10 μs. Remember that, at the CE, a fast charge recombination is preferred. Considering the great advantages of ferrocene, in terms of fast kinetic and chemical stability, its use with $Cu_{2-x}S$ CEs should be considered in DSSC using organic or natural dyes, which commonly suffer chemical degradation in contact with I^-/I_3^-. Our method could also be considered for large-scale application because of the low toxicity and cost of the solvent (EtOH) used for the deposition.

5. Conclusions

An easy, cheap and fast method for the preparation of $Cu_{2-x}S$ CEs is hereby proposed. The CEs prepared through this method have shown a good electrocatalytic efficiency for both the reduction and oxidation of the ferrocene/ferrocenium redox couple. Both cyclic voltammetry and EIS measurements have shown an electrochemical behaviour similar to that observed using the most expensive Pt CEs, presenting low values of charge transfer resistance at the interface with the redox electrolyte. The CEs have shown high stability under electrochemical stressing conditions. We suggest $Cu_{2-x}S$ CEs for solar cell applications using ferrocene-based electrolytes. In fact, this material could be a cheap alternative to the common used Pt in dye solar cells using ferrocene as redox shuttle.

Acknowledgements

This work was supported by FAPESP (Fundação de Amparo à Pesquisa do Estado de São Paulo), Processo FAPESP 2013/07396-7 and 2011/21830-6. CEPID FAPESP 2013/57872-1. AFM imaging and processing by PhD Yendry Corrales Ureña. We thank Professor Fenelon Martinho Lima Pontes for the help in the realization of XRD measurements. We especially thank the department of Chemistry of the University of Rome "La Sapienza" for allowing the use of its facilities.

References

[1] B. O'regan, M. Gräzel, A low-cost, high-efficiency solar cell based on dye-sensitized, Nature 353 (1991) 737–740.
[2] M. Ye, X. Wen, M. Wang, J. Iocozzia, N. Zhang, C. Lin, et al., Recent advances in dye-sensitized solar cells: from photoanodes, sensitizers and electrolytes to counter electrodes, Mater. Today 18 (2015) 155–162, http://dx.doi.org/10.1016/j.mattod.2014.09.001.
[3] S. Mathew, A. Yella, P. Gao, R. Humphry-Baker, F.E. Curchod, N. Ashari-Astani, et al., Dye-sensitized solar cells with 13% efficiency achieved through the molecular engineering of porphyrin sensitizers, Nat. Chem. 6 (2014) 242–247, http://dx.doi.org/10.1038/nchem.1861.
[4] A. Agresti, S. Pescetelli, A. Quatela, S. Mastroianni, T.M. Brown, A. Reale, et al., Micro-Raman analysis of reverse bias stressed dye-sensitized solar cells, RSC Adv. 4 (2014) 12366, http://dx.doi.org/10.1039/c3ra47797e.
[5] S. Mastroianni, A. Lembo, T.M. Brown, A. Reale, A. Di Carlo, Electrochemistry in reverse biased dye solar cells and dye/electrolyte degradation mechanisms, ChemPhysChem 13 (2012) 2964–2975, http://dx.doi.org/10.1002/cphc.201200229.
[6] M. Flasque, A.N. Van Nhien, J. Swiatowska, A. Seyeux, C. Davoisne, F. Sauvage, Interface stability of a TiO_2/3-methoxypropionitrile-based electrolyte: first evidence for solid electrolyte interphase formation and implications, ChemPhysChem 15 (2014) 1126–1137.
[7] H. Greijer, J. Lindgren, A. Hagfeldt, Resonance Raman scattering of a dye-sensitized solar cell: mechanism of thiocyanato ligand exchange, J. Phys. Chem. B 105 (2001) 6314–6320.
[8] P.E. Hansen, P.T. Nguyen, J. Krake, J. Spanget-Larsen, T. Lund, Dye-sensitized solar cells and complexes between pyridines and iodines. A NMR, IR and DFT study, Spectrochim. Acta A Mol. Biomol. Spectrosc. 98 (2012) 247–251.
[9] S.M. Feldt, E.A. Gibson, E. Gabrielsson, L. Sun, G. Boschloo, A. Hagfeldt, Design of organic dyes and cobalt polypyridine redox mediators for high-efficiency dye-sensitized solar cells, J. Am. Chem. Soc. 132 (2010) 16714–16724, http://dx.doi.org/10.1021/ja1088869.
[10] T.W. Hamann, The end of iodide? Cobalt complex redox shuttles in DSSCs, Dalton Trans. 41 (2012) 3111–3115, http://dx.doi.org/10.1039/c2dt12362b.
[11] B.M. Klahr, T.W. Hamann, Performance enhancement and limitations of cobalt bipyridyl redox shuttles in dye-sensitized solar cells, J. Phys. Chem. C 113 (2009) 14040–14045, http://dx.doi.org/10.1021/jp903431s.
[12] T. Daeneke, T.-H. Kwon, A.B. Holmes, N.W. Duffy, U. Bach, L. Spiccia, High-efficiency dye-sensitized solar cells with ferrocene-based electrolytes, Nat. Chem. 3 (2011) 211–215, http://dx.doi.org/10.1038/nchem.966.
[13] J.-L. Lan, Y.-Y. Wang, C.-C. Wan, T.-C. Wei, H.-P. Feng, C. Peng, et al., The simple and easy way to manufacture counter electrode for dye-sensitized solar cells, Curr. Appl. Phys. 10 (2010) S168–S171, http://dx.doi.org/10.1016/j.cap.2009.11.064.
[14] B. Zhang, D. Wang, Y. Hou, S. Yang, X.H. Yang, J.H. Zhong, et al., Facet-dependent catalytic activity of platinum nanocrystals for triiodide reduction in dye-sensitized solar cells, Sci. Rep. 3 (2013) 1836, http://dx.doi.org/10.1038/srep01836.
[15] S. AbdulAlmohsin, M. Mohammed, Z. Li, M.A. Thomas, K.Y. Wu, J.B. Cui, Multi-walled carbon nanotubes as a new counter electrode for dye-sensitized solar cells, J. Nanosci. Nanotechnol. 12 (2012) 2374–2379 (http://www.ncbi.nlm.nih.gov/pubmed/22755061 (accessed April 26, 2014)).
[16] I. Ahmad, J.E. McCarthy, M. Bari, Y.K. Gun'ko, Carbon nanomaterial based counter electrodes for dye sensitized solar cells, Sol. Energy 102 (2014) 152–161, http://dx.doi.org/10.1016/j.solener.2014.01.012.
[17] H. Wang, Y.H. Hu, Graphene as a counter electrode material for dye-sensitized solar cells, Energy Environ. Sci. 5 (2012) 8182, http://dx.doi.org/10.1039/c2ee21905k.
[18] S. Yun, A. Hagfeldt, T. Ma, Pt-free counter electrode for dye-sensitized solar cells with high efficiency, Adv. Mater. (2014), http://dx.doi.org/10.1002/adma.201402056.
[19] M. Congiu, L.G.S. Albano, F. Decker, C.F.O. Graeff, Single precursor route to efficient cobalt sulphide counter electrodes for dye sensitized solar cells, Electrochim. Acta 151 (2015) 517–524, http://dx.doi.org/10.1016/j.electacta.2014.11.001.
[20] J.-Y. Lin, J.-H. Liao, S.-W. Chou, Cathodic electrodeposition of highly porous cobalt sulfide counter electrodes for dye-sensitized solar cells, Electrochim. Acta 56 (2011) 8818–8826, http://dx.doi.org/10.1016/j.electacta.2011.07.080.
[21] J.-Y. Lin, J.-H. Liao, T.-C. Wei, Honeycomb-like CoS counter electrodes for transparent dye-sensitized solar cells, Electrochem. Solid-State Lett. 14 (2011) D41–D44.
[22] J. Huo, M. Zheng, Y. Tu, J. Wu, L. Hu, S. Dai, A high performance cobalt sulfide counter electrode for dye-sensitized solar cells, Electrochim. Acta 159 (2015) 166–173, http://dx.doi.org/10.1016/j.electacta.2015.01.214.
[23] M. Congiu, A. Lanuti, A. di Carlo, C.F.O. Graeff, A novel and large area suitable water-based ink for the deposition of cobalt sulfide films for solar energy conversion with iodine-free electrolytes, Sol. Energy 122 (2015) 87–96, http://dx.doi.org/10.1016/j.solener.2015.08.032.
[24] H. Pathan, J. Desai, C. Lokhande, Modified chemical deposition and physico-chemical properties of copper sulphide (Cu2S) thin films, Appl. Surf. Sci. 202 (2002) 47–56, http://dx.doi.org/10.1016/S0169-4332(02)00843-7.
[25] Y. Wu, C. Wadia, W. Ma, B. Sadtler, A.P. Alivisatos, Synthesis and photovoltaic application of copper(I) sulfide nanocrystals, Nano Lett. 8 (2008) 2551–2555, http://dx.doi.org/10.1021/nl801817d.
[26] J. Kundu, D. Pradhan, Influence of precursor concentration, surfactant and temperature on the hydrothermal synthesis of CuS: structural, thermal and optical properties, New J. Chem. 37 (2013) 1470, http://dx.doi.org/10.1039/c3nj41142g.
[27] L. Li, P. Zhu, S. Peng, M. Srinivasan, Q. Yan, A.S. Nair, et al., Controlled growth of CuS on electrospun carbon nanofibers as an efficient counter electrode for quantum dot-sensitized solar cells, J. Phys. Chem. C 118 (2014) 16526–16535, http://dx.doi.org/10.1021/jp4117529.
[28] S.-Y. Lee, M.-A. Park, J.-H. Kim, H. Kim, C.-J. Choi, D.-K. Lee, et al., Enhanced electrocatalytic activity of the annealed $Cu_{2-x}S$ counter electrode for quantum dot-sensitized solar cells, J. Electrochem. Soc. 160 (2013) H847–H851.
[29] M. Basu, A.K. Sinha, M. Pradhan, S. Sarkar, Y. Negishi, T. Pal, Evolution of hierarchical hexagonal stacked plates of CuS from liquid–liquid interface and its photocatalytic application for oxidative degradation of different dyes under indoor lighting, Environ. Sci. Technol. 44 (2010) 6313–6318, http://dx.doi.org/10.1021/es101323w.
[30] A.J. Bard, L.R. Faulkner, Electrochemical Methods: Fundamentals and Applications, Wiley, New York, 1980.
[31] Y. Zhao, H. Pan, Y. Lou, X. Qiu, J. Zhu, C. Burda, Plasmonic $Cu_{2-x}S$ nanocrystals: optical and structural properties of copper-deficient copper (I) sulfides, J. Am. Chem. Soc. 131 (2009) 4253–4261.
[32] J.B. Shi, P.F. Wu, Y.C. Chen, Y.C. Chang, M.Z. Tsai, F.C. Cheng, et al., Conversion of CuS thin films to structured nanosheet $CuyS$ $(1 < y \leqq 2)$ by vacuum annealing, Cryst. Res. Technol. 49 (2014) 860–864.
[33] J.G. Dunn, C. Muzenda, Thermal oxidation of covellite (CuS), Thermochim. Acta 369 (2001) 117–123.
[34] H. Ter Maat, J.A. Hogendoorn, G.F. Versteeg, The removal of hydrogen sulfide from gas streams using an aqueous metal sulfate absorbent: part II. The regeneration of copper sulfide to copper oxide—an experimental study, Sep. Purif. Technol. 43 (2005) 199–213.
[35] K.-T. Lee, D.-M. Liu, Y.-Y. Liang, N. Matsushita, T. Ikoma, S.-Y. Lu, Porous fluorine-doped tin oxide as a promising substrate for electrochemical biosensors-demonstration in hydrogen peroxide sensing, J. Mater. Chem. B 2 (2014) 7779–7784, http://dx.doi.org/10.1039/C4TB01191K.
[36] G. Lefèvre, J. Bessiere, J.-J. Ehrhardt, A. Walcarius, Immobilization of iodide on copper (I) sulfide minerals, J. Environ. Radioact. 70 (2003) 73–83.
[37] a. Petrocco, M. Liberatore, a. Di Carlo, a. Reale, T.M. Brown, F. Decker, Thermal activation of mass transport and charge transfer at Pt in the I(3)(−)/I(−) electrolyte of a dye-sensitized solar cell, Phys. Chem. Chem. Phys. 12 (2010) 10786–10792, http://dx.doi.org/10.1039/c002840a.
[38] M. Liberatore, F. Decker, L. Burtone, V. Zardetto, T.M. Brown, A. Reale, et al., Using EIS for diagnosis of dye-sensitized solar cells performance, J. Appl. Electrochem. 39 (2009) 2291–2295, http://dx.doi.org/10.1007/s10800-009-9806-5.
[39] P. Jasinski, V. Petrovsky, T. Suzuki, H.U. Anderson, Impedance studies of diffusion phenomena and ionic and electronic conductivity of cerium oxide, J. Electrochem. Soc. 152 (2005) J27–J32.
[40] C.O. Laoire, E. Plichta, M. Hendrickson, S. Mukerjee, K.M. Abraham, Electrochemical studies of ferrocene in a lithium ion conducting organic carbonate electrolyte, Electrochim. Acta 54 (2009) 6560–6564.
[41] M. Congiu, L.G.S. Albano, F. Decker, C.F.O. Graeff, Single precursor route to efficient cobalt sulphide counter electrodes for dye sensitized solar cells, Electrochim. Acta 151 (2015) 517–524, http://dx.doi.org/10.1016/j.electacta.2014.11.001.
[42] B. Park, M. Pazoki, K. Aitola, S. Jeong, E.M.J. Johansson, A. Hagfeldt, et al., Understanding interfacial charge transfer between metallic PEDOT counter electrodes and a cobalt redox shuttle in dye-sensitized solar cells, ACS Appl. Mater. Interfaces 6 (2014) 2074–2079, http://dx.doi.org/10.1021/am405108d.